In situ cosmogenic radiocarbon production and 2-D ice flow line modeling for an Antarctic blue ice area

Christo Buizert,[1] Vasilii V. Petrenko,[2,3] Jeffrey L. Kavanaugh,[4] Kurt M. Cuffey,[5] Nathaniel A. Lifton,[6] Edward J. Brook,[7] and Jeffrey P. Severinghaus[8]

Received 13 May 2011; revised 10 April 2012; accepted 12 April 2012; published 24 May 2012.

[1] Radiocarbon measurements at ice margin sites and blue ice areas can potentially be used for ice dating, ablation rate estimates and paleoclimatic reconstructions. Part of the measured signal comes from in situ cosmogenic ^{14}C production in ice, and this component must be well understood before useful information can be extracted from ^{14}C data. We combine cosmic ray scaling and production estimates with a two-dimensional ice flow line model to study cosmogenic ^{14}C production at Taylor Glacier, Antarctica. We find (1) that ^{14}C production through thermal neutron capture by nitrogen in air bubbles is negligible; (2) that including ice flow patterns caused by basal topography can lead to a surface ^{14}C activity that differs by up to 25% from the activity calculated using an ablation-only approximation, which is used in all prior work; and (3) that at high ablation margin sites, solar modulation of the cosmic ray flux may change the strength of the dominant spallogenic production by up to 10%. As part of this effort we model two-dimensional ice flow along the central flow line of Taylor Glacier. We present two methods for parameterizing vertical strain rates, and assess which method is more reliable for Taylor Glacier. Finally, we present a sensitivity study from which we conclude that uncertainties in published cosmogenic production rates are the largest source of potential error. The results presented here can inform ongoing and future ^{14}C and ice flow studies at ice margin sites, including important paleoclimatic applications such as the reconstruction of paleoatmospheric ^{14}C content of methane.

Citation: Buizert, C., V. V. Petrenko, J. L. Kavanaugh, K. M. Cuffey, N. A. Lifton, E. J. Brook, and J. P. Severinghaus (2012), In situ cosmogenic radiocarbon production and 2-D ice flow line modeling for an Antarctic blue ice area, *J. Geophys. Res.*, *117*, F02029, doi:10.1029/2011JF002086.

1. Introduction

[2] Ice cores from polar regions have been used to reconstruct climate variations as far as 800 ka back in time [e.g., *Jouzel et al.*, 2007]. Old ice can not only be obtained from deep ice cores, but also at ice margins and Antarctic blue ice areas (BIAs) where it is re-exposed by ablation [*Reeh et al.*, 2002; *Bintanja*, 1999]. For paleoclimate studies this provides an interesting alternative to ice coring, as sample retrieval is less challenging from both technological and logistical points of view. Old ice can be sampled from near the surface, making the method especially well suited for experiments that require large ice samples [*Petrenko et al.*, 2009]. Dating of ice parcels is the principal problem when using ablation sites for climatic reconstruction [*Sinisalo and Moore*, 2010, and references therein]. Several methods have been used, including radiometric dating of tephra layers [e.g., *Dunbar et al.*, 2008], flow line modeling [*Azuma et al.*, 1985; *Grinsted et al.*, 2003; *Moore et al.*, 2006], stratigraphical matching of gas and water isotope measurements to well-dated ice core records [e.g., *Reeh et al.*, 2002; *Petrenko et al.*, 2006; *Aciego et al.*, 2007; *Schaefer et al.*, 2009], and radiocarbon dating of micro-particles [*Jenk et al.*, 2007]. Early on it was realized that radiocarbon dating of the CO_2 present in the air bubbles trapped in polar ice can potentially be used as an absolute dating method for ice cores and BIA samples [*Fireman and Norris*, 1982; *Andree et al.*, 1984]. In this method the air is extracted from the ice sample, after which the CO_2 is isolated for ^{14}C

[1]Centre for Ice and Climate, Niels Bohr Institute, University of Copenhagen, Copenhagen, Denmark.
[2]Institute of Arctic and Alpine Research, University of Colorado, Boulder, Colorado, USA.
[3]Now at Department of Earth and Environmental Sciences, University of Rochester, Rochester, New York, USA.
[4]Department of Earth and Atmospheric Sciences, University of Alberta, Edmonton, Alberta, Canada.
[5]Department of Geography, University of California, Berkeley, California, USA.
[6]Earth and Atmospheric Sciences department, Purdue University, West Lafayette, Indiana, USA.
[7]Department of Geosciences, Oregon State University, Corvallis, Oregon, USA.
[8]Scripps Institution of Oceanography, University of California, San Diego, La Jolla, California, USA.

Corresponding author: C. Buizert, Centre for Ice and Climate, Niels Bohr Institute, University of Copenhagen, Juliane Maries vej 30, DK-2100 Copenhagen, Denmark.

0148-0227/12/2011JF002086

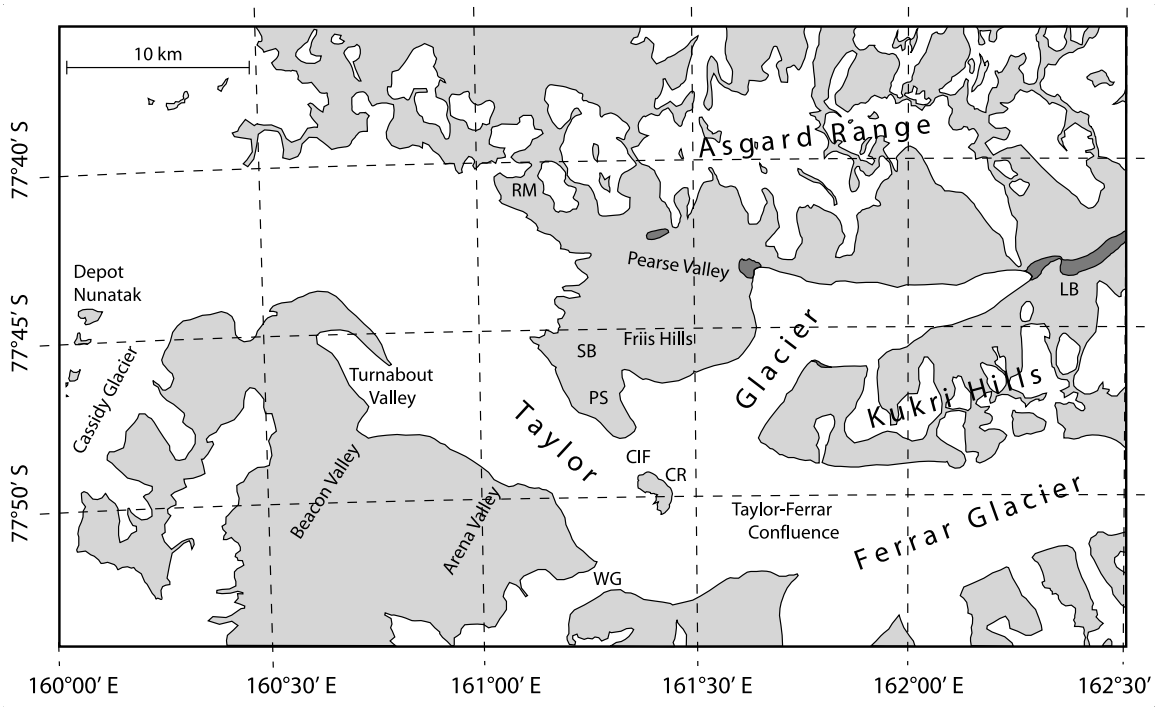

Figure 1. The Taylor Glacier with surroundings. Abbreviations are Round Mountain (RM), Simmons Basin (SB), Pandora Spire (PS), the Cavendish Ice Falls (CIF), Cavendish Rocks (CR), Windy Gully (WG), and Lake Bonney (LB).

analysis. Interpretation of the ^{14}C data, however, is complicated by cosmogenic in situ production of ^{14}C from oxygen atoms found in ice [*Lal et al.*, 1990]. When this effect is corrected for, the air bubbles contained in the ice can be dated with an accuracy of a few thousands of years [*Van de Wal et al.*, 1994; *Van Roijen et al.*, 1995; *Van Der Kemp et al.*, 2002; *De Jong et al.*, 2004; *Van de Wal et al.*, 2007].

[3] Apart from dating applications, there are other reasons for studying radiocarbon in ice. First, surface ^{14}C concentrations (in either ^{14}CO or $^{14}CO_2$) reflect ablation (or accumulation) rates at the site under study. At sites with low ablation rates the ice parcels move slowly through the top ~5 m (where cosmogenic irradiation is strongest), leading to a high surface ^{14}C activity because the cosmogenic ^{14}C accumulates over time. The opposite is also true: where ablation rates are high, activity will be low. By this principle, measurements of ^{14}C have been used to estimate BIA ablation rates [e.g., *Lal et al.*, 1990; *Van Roijen et al.*, 1995; *Van der Borg et al.*, 2001]. It has also been suggested that ^{14}C in ice core samples can be used to infer past changes in accumulation rate [*Lal et al.*, 1990, 2000].

[4] Second, at well-dated ablation sites paleoclimate information can be obtained from radiocarbon measurements. Fossil carbon sources are depleted in ^{14}C, and in this way measuring the ^{14}C activity of carbon-containing gas species can teach us about the fossil contribution to their past atmospheric variations. In particular, the ^{14}C variations in methane (CH_4) over the last glacial termination contain information on how much the destabilization of ^{14}C-depleted methane hydrates contributed to the observed CH_4 increases [*Petrenko et al.*, 2008, 2009].

[5] Measurable amounts of cosmogenic ^{14}C are produced down to a depth of ~200 m below the ice surface, and consequently the ice flow at the sampling site must be well understood to correctly interpret ^{14}C data. The aim of this study is to investigate the influence of ice flow on cosmogenic ^{14}C production. Our study site is Taylor Glacier, Antarctica – an outlet glacier of the East Antarctic Ice Sheet that originates at Taylor Dome, and terminates in the McMurdo Dry Valleys (Figure 1). Over much of the glacier's length, ablation exceeds accumulation; as such, the lower reaches of the glacier are a BIA. Ablation is dominated by sublimation [*Bliss et al.*, 2011]; current ablation rates are around 0.1–0.3 m a^{-1}, which is typical of Antarctic BIAs [*Bintanja*, 1999].

[6] Taylor Glacier presents an interesting study case for several reasons. First, it has been the subject of an extensive recent glaciological survey [*Kavanaugh and Cuffey*, 2009; *Kavanaugh et al.*, 2009a, 2009b], providing the data required to reliably model the ice flow. Second, the glacier flows through a region of rugged topography. This is representative of Antarctic BIAs, many of which are found in close proximity to mountain ranges and nunataks [*Bintanja*, 1999; *Sinisalo and Moore*, 2010]. Finally, the site is of interest to paleoclimatic studies because the exposed ice has ages between approximately 11.5 and 65 ka [*Aciego et al.*, 2007]. In particular the large (~1000 kg) ice samples required for high precision ^{14}C measurements of CH_4 can be obtained from near the glacier surface [*Petrenko et al.*, 2008].

[7] In this work we combine 2-D flow line modeling with comprehensive cosmogenic exposure theory to obtain a best estimate for the ^{14}C activity of ablating Taylor Glacier ice.

Table 1. Constants Used in ^{14}C Production Calculations

Mechanism i	Λ_i (g cm^{-2})	P_i^{0a} (g^{-1} a^{-1})	Λ_i/ρ^b (m)
Neutrons	150[c]	30.7 ± 5[d]	1.6
Muon capture	1510[d]	4.75 ± 0.4[d]	16.4
Fast muons	4320[e]	0.74 ± 0.4[d]	47.1

[a]At sea level and high latitude.
[b]^{14}C production e-folding depth in ice.
[c]*Lal et al.* [1987]; *Van de Wal et al.* [2007].
[d]*Heisinger et al.* [2002a].
[e]*Heisinger et al.* [2002b].

The combined model allows us to assess the influence of basal topography and solar modulation on the cosmogenic ^{14}C production; we demonstrate under which conditions these two effects become significant enough to deserve consideration. We furthermore show production by thermal neutron capture to be negligible under all conditions. Although our focus is primarily on Taylor Glacier, these conclusions are applicable to all studies of ^{14}C in ice cores and BIAs.

[8] The model also has applications that are very specific to forthcoming ^{14}C samples from Taylor Glacier. During a 2010/2011 austral summer field campaign, samples for radiocarbon analyses were taken at Taylor Glacier with the purpose of better constraining in situ production rates. We will show that at the sampling location the influence of ice flow strain rates on ^{14}C activity is minimal, greatly simplifying data interpretation. More importantly, the model will serve as a framework for correcting $^{14}CH_4$ measurements over the abrupt methane increases observed for the last glacial termination for the effects of in situ production, with the purpose of reconstructing of the true paleo-atmospheric signal.

2. Cosmogenic Production of ^{14}C in Ice

[9] Cosmic rays consist largely of charged subatomic particles originating from outside the Earth's magnetosphere. Upon entering the upper atmosphere, particles of sufficient energy cause nuclear disintegrations, from which a shower, or cascade, of secondary cosmic ray particles is produced. On interacting with the materials of Earth's surface, these secondary cosmic rays are capable of producing a wide variety of terrestrial cosmogenic nuclei (TCN) (see *Gosse and Phillips* [2001, and references therein] for an overview of TCN exposure theory). In ice, ^{14}C is produced cosmogenically, primarily through neutron spallation of oxygen atoms [*Lal et al.*, 1990]. After production, the ^{14}C atoms are predominantly oxidized to form either $^{14}CO_2$ or ^{14}CO. The reported fraction of ^{14}CO out of the total in situ ^{14}C ranges from 0.20–0.57 (the remainder being $^{14}CO_2$) [*Lal et al.*, 1990; *Van Roijen et al.*, 1995; *Lal et al.*, 2000; *Van Der Kemp et al.*, 2002; *De Jong et al.*, 2004]. A recent study, however, suggests $^{14}CH_4$ is formed in small amounts as well [*Petrenko et al.*, 2009].

[10] Ice found in BIAs has experienced two intervals of exposure: one in the accumulation zone and one during ablation. Interpretation of the ablation signal is more straightforward because all the cosmogenic ^{14}C is retained. In the accumulation zone, the presence of a ventilated porous firn layer complicates interpretation. Given the results published to date, it is unclear how much , if any, of the ^{14}C that is produced in the accumulation zone is actually retained [e.g., *Smith et al.*, 2000; *Lal et al.*, 2001; *De Jong et al.*, 2004; *Van de Wal et al.*, 2007]. We focus our attention on ^{14}C production in the ablation zone. For ice older than ~50 ka, essentially all of the accumulation-zone cosmogenic ^{14}C will have decayed, and only ablation-zone production is of importance. For younger ice inheritance will need to be considered separately.

[11] We will consider four different mechanisms of in situ cosmogenic ^{14}C production in ice. Three of these involve nuclear reactions with oxygen; the fourth involves the capture of thermal neutrons by the nitrogen present in the air bubbles found in glacial ice.

2.1. Spallogenic and Muogenic Production

[12] We first consider neutron spallation reactions [*Lal et al.*, 1990, 2000], negative muon capture [*Van der Borg et al.*, 2001; *Van Der Kemp et al.*, 2002; *Heisinger et al.*, 2002a], and fast muon reactions [*Heisinger et al.*, 2002b; *Nesterenok and Naidenov*, 2009]. The neutron and muon fluxes incident on the glacier surface are attenuated in the ice, giving a production rate $P(z)$ that falls off with depth following

$$P_i(z) = P_i^0 e^{-Z/\Lambda_i} = P_i^0 e^{-\rho z/\Lambda_i} \quad (1)$$

where P_i^0 is the surface production rate, Z the overburden in g cm^{-2}, z the depth in cm, Λ_i the absorption mean free path in g cm^{-2}, and ρ the density of the medium (for ice we use ρ = 0.92 g cm^{-3}). Following *Heisinger et al.* [2002a], the subscript i can take the values h, μ^- and μ_f to denote neutron spallation (also referred to as the hadronic component), negative muon capture, and fast muons, respectively. The production constants used in this study are summarized in Table 1, where the last column gives the e-folding depth for each production mechanism. Figure 2a shows the decrease of production rate with depth.

[13] Following convention, surface production rates are listed at sea level and at high latitude. At elevation there is less shielding by the overlying atmosphere, giving an increased cosmic ray flux and radionuclide production. At low latitudes, the Earth's magnetic field shields more of the incoming rays, leading to lower nuclide production. To incorporate both effects, scaling relations are used, which give nuclide production rates at any point at the Earth's surface relative to the reported high latitude sea level production rates [*Lal*, 1991; *Dunai*, 2000; *Gosse and Phillips*, 2001; *Desilets and Zreda*, 2003; *Desilets et al.*, 2006; *Lifton et al.*, 2005]. We use the scaling model of *Lifton et al.* [2005], which provides the most detailed description of muogenic scaling factors based on muon monitor data covering a wide range of altitudes and latitudes. Furthermore, the Lifton scaling model includes the effect of solar modulation, which can alter the spallogenic production by ~10% at the high geomagnetic latitudes of our study site (Section 4.2).

[14] The altitude dependence is described by the atmospheric depth X (in g cm^{-2}), which equals the mass of the overlying atmosphere traversed by the incident cosmic rays at a given elevation. Note that X is directly proportional to

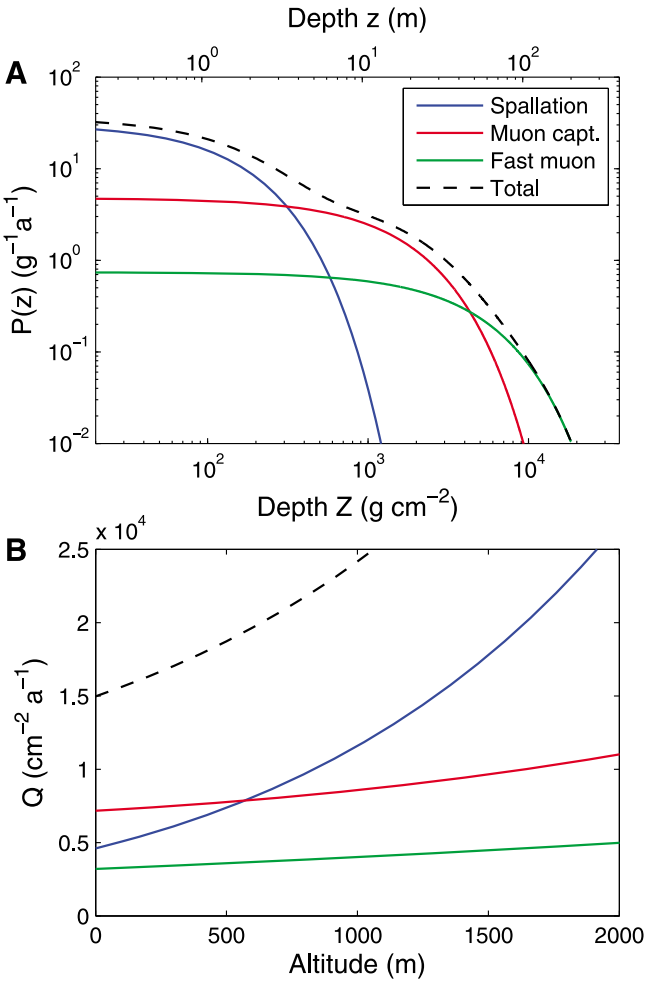

Figure 2. (a) In situ ^{14}C production rates with depth below the glacier surface, using equation (1) and the values listed in Table 1. The glacier surface is taken at sea level. The black dashed line represents the sum of the individual mechanisms. (b) Altitude dependence of the production using the *Lifton et al.* [2005] model. The colors represent the three mechanisms; the vertical axis shows the integrated production $Q_i = \int_0^\infty P_i(z)dz$.

the barometric pressure. Radionuclide studies often use the standard atmosphere as a basis for relating pressure to altitude [*Lal*, 1991]. This works well in midlatitudes, but because atmospheric pressure at a given elevation decreases with increasing latitude this underestimates the cosmic ray flux over Antarctica. Therefore we use the pressure-altitude relation over Antarctica from *Stone* [2000]. The latitudinal dependence of the cosmic ray flux is described by the effective vertical cutoff rigidity R_C, which is a measure of the threshold energy required for a (charged) cosmic ray particle to access a given point within the Earth's magnetosphere. R_C is inversely related to the geomagnetic latitude, and the scaling model is latitude invariant at geomagnetic latitudes greater than approximately ~60° S, equivalent to $R_C \leq 1.9$ [*Lifton et al.*, 2005]. Taylor Glacier falls within this latitude range, and therefore we let $R_C = 0$. Figure 2b shows how the integrated ice column production $Q_i = \int_0^\infty P_i(Z)dZ$ changes with altitude. The integrated production Q_i scales linearly with the surface production rate P_i^0, but is more informative since it shows the total amount of in situ ^{14}C produced in the ice column. Spallogenic production shows a more pronounced altitude dependence than muogenic production, because the neutron flux is more strongly attenuated by the atmosphere than the muon fluxes are.

2.2. Thermal Neutron Capture

[15] Glacial ice contains a finite amount of trapped air, typically about 0.1 mL g^{-1} at standard temperature and pressure (STP). The final mechanism of ^{14}C production we consider is absorption of thermal neutrons by the nitrogen (N_2) present in gas bubbles, following the ^{14}N(n, p)^{14}C nuclear reaction pathway. This is the dominant mechanism for radiocarbon production in the atmosphere. To the best of our knowledge, this mechanism has been ignored to date in studies of radiocarbon production in ice. In this section we implement a simple neutron flux model to estimate the ^{14}C production rate by thermal neutron absorption.

[16] Low-energy neutrons, such as thermal neutrons, originate from fast (spallogenic) neutrons whose energy has been moderated through interaction with matter [*Gosse and Phillips*, 2001]. On slowing down they first pass through the epithermal energy range (0.5 eV < E_n < 1 keV, with E_n the neutron energy), and subsequently the thermal energy range (0 < E_n < 0.5 eV), where neutron energy is on the order of the thermal vibrations of their surroundings. At these energies they can no longer lose their energy by momentum transfer to incident nuclei, and the only sink mechanisms to the thermal neutron flux are capture and free neutron decay.

[17] To calculate both the epithermal and thermal neutron fluxes near the ice-atmosphere interface, we use a model by *Phillips et al.* [2001]. Table 2 gives the low-energy transport parameters used here, where for each element k we list its mass A, average log decrement of energy loss per collision ξ, epithermal neutron scattering cross-section σ_{sc}, thermal neutron capture cross-section σ_{th} and the dilute resonance integral for absorption of epithermal neutrons I_a. We also list the estimated concentrations in atoms per gram of the different elements for both ice and atmosphere (N_{ice} and N_{atm}, respectively). The low-energy neutron model is first verified by comparing the calculated fluxes to measured fluxes in a block of concrete at Los Alamos National Laboratory, USA [*Liu et al.*, 1994]. The model reproduces the observations within 10%, giving us confidence that, at the very least, the model will calcluate the fluxes to the correct order of magnitude. Figure 3a shows the calculated epithermal and thermal fluxes (Φ_{eth} and Φ_{th}, respectively) for an ice-atmosphere interface at sea level. We see that the epithermal flux in the ice is strongly reduced. This is due to the presence of hydrogen as the most abundant element, which is a very effective moderator of epithermal neutrons (Table 2).This strong moderation of epithermal neutrons leads to a sharp increase in the thermal neutron flux over the atmosphere-ice interface.

[18] From the calculated flux Φ_{th} we can derive the production rate of ^{14}C by thermal neutrons as

$$P_{th}(Z) = \sigma_{th,N} N_{ice,N} \Phi_{th}(Z) \quad (2)$$

Table 2. Low-Energy Neutron Transport Parameters[a]

k	A (gmol^{-1})	ξ (unitless)	σ_{sc} (10^{-24} cm^2)	σ_{th} ($^{-24}$ cm^2)	I_a (10^{-24} cm^2)	N_{ice} (10^{20} g^{-1})	N_{atm} (10^{20} g^{-1})
H	1	1	20.5	0.33	0	667	0
N	14	0.14	11.5[b]	1.9[c]	0.034[d]	0.0456	325
O	16	0.12	3.76	0.0002	0.0004	334	87.1
Ar	39.9	0.049	0.68[b]	0.675[b]	0.41[d]	0.0027	1.94

[a]Values from *Phillips et al.* [2001] unless indicated differently.
[b]*Sears* [1992].
[c]*Wagemans et al.* [2000].
[d]*Mughabghab et al.* [1992].

This is shown in Figure 3b together with the curve

$$P_{th}^{AS}(Z) = \sigma_{th,N} N_{ice,N} \Phi^{*}_{th,ice} e^{-Z/\Lambda_h} \quad (3)$$

toward which $P_{th}(Z)$ approaches asymptotically as $Z \rightarrow \infty$. The value of $\Phi^{*}_{th,\ ice}$ is given by *Phillips et al.* [2001, equation 21]. From equation (3) it is clear that to first approximation the thermal neutron production has the same depth dependence as the production by neutron spallation (equation (1)); however, the surface production rate (and thereby the integrated column production) is more than 2 orders of magnitude smaller. We shall therefore neglect ^{14}C production by thermal neutrons in the remainder of this work. Since all thermal neutrons are ultimately captured by nuclei of the host material, one might wonder why the ^{14}C production rate is so small. On comparing the values in Table 2 it is clear that hydrogen absorbs the vast majority of thermal neutrons by virtue of its abundance and relatively large capture cross-section.

3. Taylor Glacier 2-D Flow Line Modeling

[19] The ^{14}C activity of old ice in a BIA is a function of its cosmogenic exposure history, and thereby its flow path. At Taylor Glacier the individual ice parcels move both down valley, as well as toward the glacier surface due to ablation of overlying ice. In this section we present a 2-D ice flow line model for Taylor Glacier with the objective of reconstructing the trajectory of ice parcels.

3.1. Data Input to the Ice Flow Model

[20] The 2-D ice flow line modeling presented here is based on a recent series of detailed studies of the dynamics and mass balance of Taylor Glacier [*Kavanaugh and Cuffey*, 2009; *Kavanaugh et al.*, 2009a, 2009b]. From these studies we use the surface and basal digital elevation models, surface velocities obtained from both satellite radar interferometry (InSAR) and Global Positioning System (GPS) measurements of the displacement of a network of survey poles, ice-surface ablation rates, and modeled horizontal velocity profiles with depth.

[21] Figure 4 shows the outline of the glacier, with the color scale depicting the surface flow speeds used in the ice flow modeling. The red curve indicates the flow path along which we shall calculate the exposure history of ablating ice parcels. We let x be the flow-parallel coordinate with the origin at the terminus, y be perpendicular to the flow and z be the depth coordinate with $z = 0$ at the glacier surface. The distance x (in km) is indicated with red markers in Figure 4. The central flow line is constructed in two steps. The first part from $0 < x \leq 40.5$ km follows the sampling transect of a 2009–2010 field campaign, the aim of which was to accurately date the ablating ice. For $x > 40.5$ km we invert the surface velocity field and trace back an imaginary ice parcel. The flow line crosses two narrow regions of missing data around $x = 53$ km; in these locations we adjust the path by eye to obtain a smooth transition between the trajectories on both sides.

[22] The ablation rate measurements are described by *Kavanaugh et al.* [2009b]. We select poles along the center flow line as shown in Figure 4. The poles were planted during the 2002/2003 austral summer field season, and measured during the 2003/2004 season. The majority of poles relevant for this study were remeasured in the 2006/2007 season. We include additional data for 17 poles that

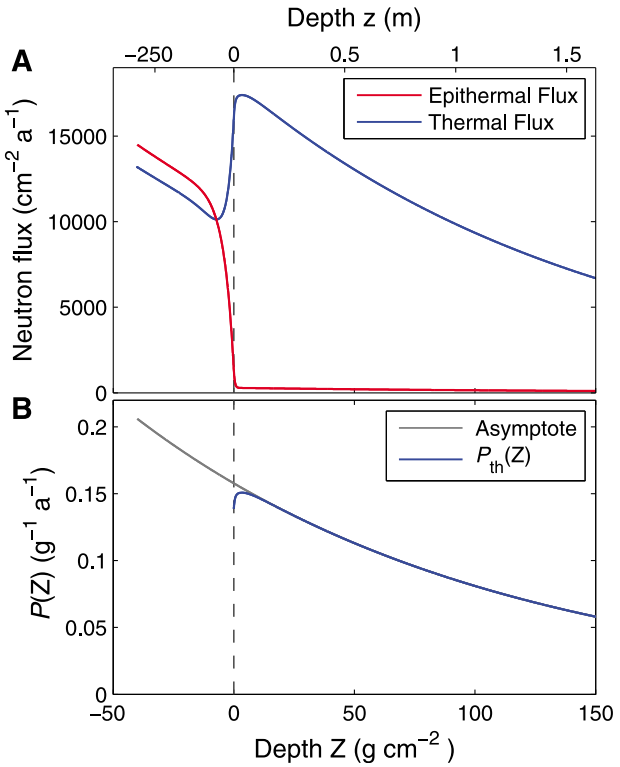

Figure 3. (a) Modeled thermal and epithermal neutron fluxes at the atmosphere-ice interface at high latitude ($R_C = 0$) and sea level. The ice surface is placed at $Z = 0$; for $Z < 0$ we have atmosphere, for $Z \geq 0$ ice. (b) Production rate of ^{14}C through the ^{14}N(n, p)^{14}C nuclear reaction given the calculated neutron fluxes, together with the asymptote given by equation (3).

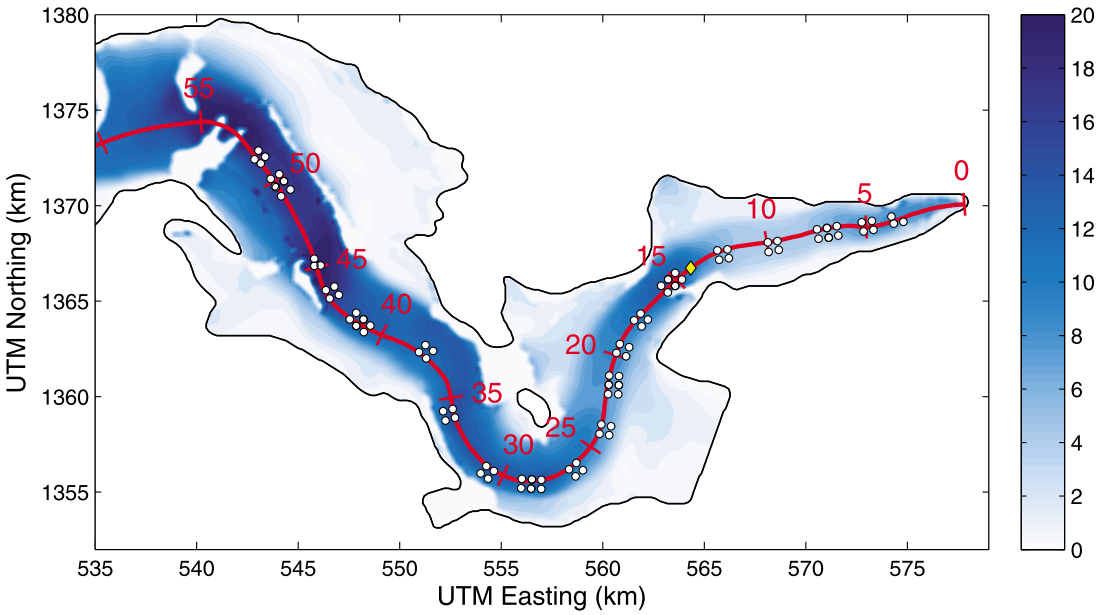

Figure 4. Color plot of glacier surface velocity in m a^{-1} from InSAR remote sensing [*Kavanaugh et al.*, 2009a]. Regions with missing data show up as light patches; here high surface deformation due to strain rates precludes phase unwrapping. White dots indicate survey poles used in this study, which are a subset of the stake network of *Kavanaugh et al.* [2009a], selected for their proximity to the center-line flow path. Ablation rate measurements as well as GPS velocity measurements are available for these poles. The red line with distance markers (in km from terminus) indicates the center flow line used in this study, the black line shows the glacier edge. The main ^{14}C sampling site of the 2010/2011 austral summer field campaign (77.762° S, 161.720° E, or x = 14.05 km) is indicated with a yellow diamond.

were remeasured during the 2009/2010 and 2010/2011 field seasons. Consequently we have ablation rate estimates averaged over 1 and 4 years for the majority of the poles, and averaged over 7 or 8 years for 17 of the poles. Due to annual variability in ablation rates the 1-year estimates differ significantly from the 4-year estimates for all poles, with the former being 4.7 cm a^{-1} more rapid on average [*Kavanaugh et al.*, 2009b]. The 4-year estimates agree well with the and 7- and 8-year averages. For each pole we take the longest available measurement period as a best estimate. For 7 poles (all at $x > 50$ km) this period equals one year; their ablation estimate is adjusted by subtracting 4.7 cm a^{-1}. The single year ablation offset from the long term average gives an estimate of the year to year variability; as an ablation rate uncertainty estimate we use 4.7 cm a^{-1} divided by $\sqrt{N}$, where N is the observation period in years (N = 1, 4, 7, 8). Pole positions are projected perpendicularly onto the flow line; poles with their x coordinates less than 200 m apart are averaged. Between stakes we use linear interpolation of both ablation rates and uncertainty estimates. The ablation rates along the glacier are shown in Figure 5a. The peak near x = 30 km is caused by strong katabatic winds coming down Windy Gully (Figure 1).

3.2. Calculating Vertical Ice Velocities Relative to the Surface

[23] To trace the trajectories of ice parcels downward back into the glacier, we need to calculate flow velocities in the x, z-plane. Let u, v, w be the velocity components along x, y, z; $\mathbf{u}$ = (u, v) the horizontal velocity vector, $\mathbf{u}_s$ = (u_s, v_s) the horizontal velocity vector at the glacier surface, and H the total ice thickness. The component w is the vertical velocity relative to the glacier surface, with positive w being flow toward the bed. We write the horizontal velocity as [*Azuma et al.*, 1985; *Grinsted et al.*, 2003; *Kavanaugh and Cuffey*, 2009]:

$$\begin{aligned} u(z) &= f(z)u_s \\ v(z) &= f(z)v_s = 0 \end{aligned} \tag{4}$$

where $f(z)$ is a scaling function which equals unity at the surface $f(0)$ = 1. *Kavanaugh and Cuffey* [2009] concluded that Taylor Glacier is frozen to the bed; for this reason we include no basal sliding ($f(H)$ = 0). We use the numerically solved scaling functions by *Kavanaugh and Cuffey* [2009] at six points along the flow line, and use linearly interpolated profiles in between. The profiles are accurate since they are based on the actual stresses and estimated temperature profiles in Taylor Glacier. Three other shapes of $f(z)$ were also tested; see Figure 5c for details.

[24] Let $\dot{b}$ denote the surface mass balance in m a^{-1}, with $\dot{b} > 0$ ($\dot{b} < 0$) indicating accumulation (ablation). The vertical velocity at the surface equals $w_s = \dot{b}$. At finite depth w (z) is given by

$$w(z) = \dot{b} + \int_0^z \dot{\varepsilon}_{zz}(z')dz' \tag{5}$$

where $\dot{\varepsilon}_{zz}$ is the vertical strain rate $\dot{\varepsilon}_{zz} = \partial w/\partial z$. We will compare two methods to estimate $\dot{\varepsilon}_{zz}$.

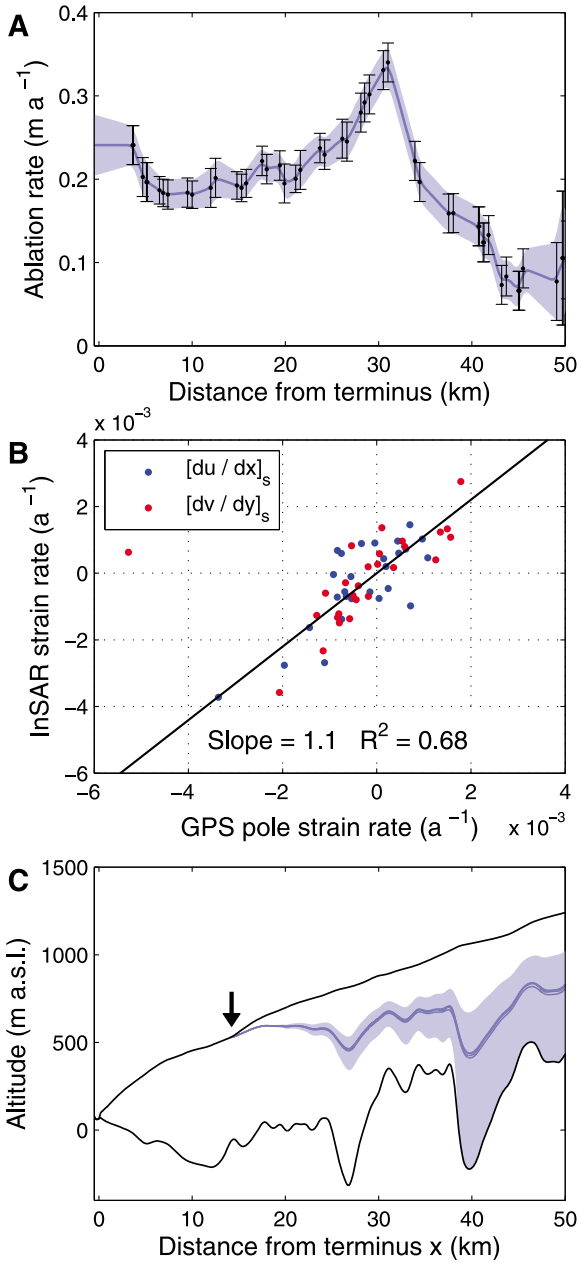

Figure 5. (a) Ablation rates from stake measurements (black dots with error bars) [*Kavanaugh et al.*, 2009b] together with the interpolated best estimate (blue line) and uncertainty estimate (light blue shading). (b) Comparison of surface strain rates estimates obtained from the GPS stake network (horizontal axis) [*Kavanaugh et al.*, 2009a] and through remote sensing (vertical axis). Outlier on left rejected in the slope fitting. (c) Uncertainty in parcel trajectory reconstruction, with glacier surface and bed (solid black lines) and 2010/2011 sampling site (arrow). Shaded region is bordered by highest- and lowest-elevation trajectories, generated using $\dot{\varepsilon}_{zz} \pm = \max(0.2 \times |\dot{\varepsilon}_{zz}|, 4.0 \times 10^{-4}\ \mathrm{a}^{-1})$. Solid blue lines show four choices of $f(z)$: (1) numerically solved profiles from *Kavanaugh and Cuffey* [2009], (2) glacial plug flow, or $f(z) = 1$, and (3), (4) $f(z) = \tanh(kz/H)/\tanh(k)$, with $k = 4$ and $k = 5$, respectively [*Grinsted et al.*, 2003]. The blue lines fall on top of each other, showing the trajectory reconstruction to be insensitive to the choice of $f(z)$.

3.2.1. Estimating $\dot{\varepsilon}_{zz}$ Using Mass Conservation in the Ice Column

[25] *Kavanaugh et al.* [2009b] have estimated that within the accuracy of their method, Taylor Glacier is in steady state. Under this assumption ($\partial H/\partial t = 0$), mass conservation in the ice column can be written as [*Cuffey and Paterson*, 2010]

$$H(\nabla \cdot \bar{\mathbf{u}}) + \bar{\mathbf{u}} \cdot (\nabla H) = \dot{b} \tag{6}$$

where $\bar{\mathbf{u}}$ is the depth-averaged horizontal velocity. We introduce the commonly used assumption that the horizontal strain rates scale the same way with depth as the horizontal velocity [*Grinsted et al.*, 2003; *Kavanaugh and Cuffey*, 2009]

$$\begin{aligned} \dot{\varepsilon}_{xx} &= \frac{\partial u}{\partial x} = f(z)\frac{\partial u_s}{\partial x} \\ \dot{\varepsilon}_{yy} &= \frac{\partial v}{\partial y} = f(z)\frac{\partial v_s}{\partial y} \end{aligned} \tag{7}$$

This is not always a good assumption near the bed, but works well for the near-surface flow that is relevant to cosmogenic production estimation. Using the fact that on the center flow line the transverse velocity $v_s = 0$ we can rewrite equation (6) as

$$H\bar{f}\left(\frac{\partial u_s}{\partial x} + \frac{\partial v_s}{\partial y}\right) + \bar{f}u_s\frac{\partial H}{\partial x} = \dot{b} \tag{8}$$

where $\bar{f}$ is the column average $\bar{f} = \frac{1}{H}\int_0^H f(z)dz$. Equation (8) assumes that $\partial\bar{f}/\partial x$ can be neglected. Using the incompressibility of ice we can solve for the vertical strain rate

$$\dot{\varepsilon}_{zz}(z) = \frac{f(z)}{H}\left(u_s\frac{\partial H}{\partial x} - \frac{\dot{b}}{\bar{f}}\right) \tag{9}$$

Note that this approach is similar to the one developed by *Grinsted et al.* [2003]; the main difference is the inclusion of the $u_s\partial H/\partial x$ term on the right hand side of equation (9), which is neglected in the cited study. For Taylor Glacier we cannot neglect this term, as there are large longitudinal variations in glacier thickness. To calculate vertical velocities with this approach, we use measurements of (1) surface mass balance (i.e., ablation rates), (2) horizontal velocity field (u_s, v_s), and (3) ice thickness H along the flow line. We also use the scaling functions $f(z)$ as derived by *Kavanaugh and Cuffey* [2009].

[26] This method does not ensure that $w(H) = 0$. After calculating $w(z)$ using equations (5) and (9) we have forced the ice near the base ($0.8H < z < H$) to transition smoothly toward flow parallel to the bed, or $w(z) = \partial H/\partial x \cdot u(z)$. Note that because the ^{14}C production happens in the upper part of the column only, this will not significantly influence our results.

3.2.2. Estimating $\dot{\varepsilon}_{zz}$ From Measured Surface Strain Rates

[27] As an alternative approach we calculate vertical strain from estimates of horizontal strain rates derived from InSAR and GPS surface flow velocities. Let $\dot{\varepsilon}^M_{xx,s}$ and $\dot{\varepsilon}^M_{yy,s}$ be the longitudinal and transverse surface strain rate estimates

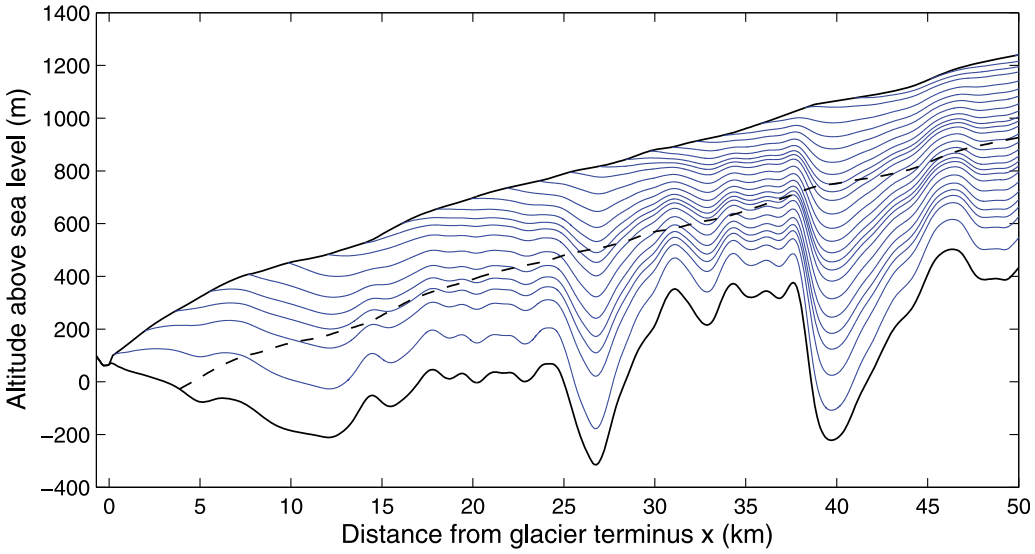

Figure 6. Modeled ice parcel trajectories along the center flow line. Model time step of 1 yr; parcels are traced 20 ka back in time. The dashed line indicates the 10 atoms g^{-1} equilibrium depth.

from measurements of $\mathbf{u}_s$. Using equation (7) and the incompressibility of ice we obtain

$$\dot{\varepsilon}_{zz}(z) = -\left(\dot{\varepsilon}^M_{xx,s} + \dot{\varepsilon}^M_{yy,s}\right) f(z) \tag{10}$$

The reliability of this approach depends on the accuracy of the surface strain rate estimates. Figure 5b shows a comparison between strain rate estimates based on the InSAR and GPS data. We see that the slope of the correlation deviates significantly from unity; that there is one clear outlier in the transverse strain rate $\dot{\varepsilon}_{yy}$; that there is much scatter in the data (R^2 = 0.68 when ignoring the outlier); and that for ~20% of the points the sign is reversed. In equation (10) the horizontal strain rates are added. By doing so the potential for error is increased further, as their uncertainties also add up.

[28] When calculating ice flow trajectories based on vertical velocities from this second approach, we find that they fail to follow bedrock undulations as required. Furthermore, mass conservation is violated as ice parcels emerge from, and disappear into, the bed. Because the trajectories fail to follow topological features, an ad-hoc adjustment (as used in the first method) cannot be applied, because it leads to sharp kinks in the flow trajectories and violations of ice continuity. For the reasons outlined above, we will use the first method (mass conservation in the ice column) to estimate ice parcel trajectories in the remainder of this study.

3.3. Tracing Ice Parcels

[29] We calculate the (u, w) velocity field in the x, z-plane at a spatial resolution of Δz = 5 m and Δx = 100 m. Using a time step Δt = 1 yr we trace parcels back into the glacier, where we use linear 2-D interpolation of (u, w) to find the velocity at each newly calculated position. The result is plotted in Figure 6. The dashed line indicates the depth where cosmogenic production and radioactive decay balance out to give a ^{14}C concentration of 10 atoms g^{-1} to hypothetical ice parcels staying at that depth indefinitely. Since surface values are on the order of 1000 atoms ^{14}C g^{-1}, any errors in the trajectory calculation below this line can introduce at most a 1% error in calculated surface values.

[30] Any choice of strain rate parameterization introduces an error. To assess the potential for error, we introduce two extreme flow cases acting as an uncertainty envelope to the true flow path. This is depicted in Figure 5c. The shaded region is bordered by the two envelope scenarios, which are calculated by using $\dot{\varepsilon}_{zz} \pm \sigma_{\dot{\varepsilon}_{zz}}$ in equation (5), where the strain rate uncertainty is arbitrarily set to $\sigma_{\dot{\varepsilon}_{zz}} = \max(0.2 \times |\dot{\varepsilon}_{zz}|, 4.0 \times 10^{-4}\ \mathrm{a}^{-1})$. We expect the true flow path to lie within the shaded area enveloped by these two extreme flow cases that represent a highest- and lowest elevation trajectory. We will use this uncertainty envelope in the sensitivity study presented in section 4.3. We furthermore test four different choices of the shape function $f(z)$, which are plotted as the blue solid trajectories in Figure 5c. Note that the curves cannot be distinguished easily, because the four trajectories differ very little. It is clear that any uncertainty in $f(z)$ is of lesser importance, and is included within the flow envelope.

4. Results and Discussion

4.1. Taylor Glacier ^{14}C Estimates

[31] Knowing the path ($x(t)$, $z(t)$) of an ice parcel back in time allows us to calculate the time evolution of the cosmogenically produced ^{14}C concentration:

$$\begin{aligned} \frac{d\left[^{14}\mathrm{C}\right]_i}{dt} &= P_i^0(x(t)) e^{\rho z(t)/\Lambda_i} - \lambda \left[^{14}\mathrm{C}\right]_i \\ \left[^{14}\mathrm{C}\right]_i(t) &= A_i + \int_0^t \frac{d\left[^{14}\mathrm{C}\right]_i}{dt'} dt' \end{aligned} \tag{11}$$

Here $[^{14}\mathrm{C}]_i$ denotes the concentration of ^{14}C in atoms g^{-1} produced by cosmogenic mechanism i, λ is the decay constant (1/8267 a^{-1}), and A is the inheritance from previous cosmogenic exposure (e.g., in the accumulation zone). The

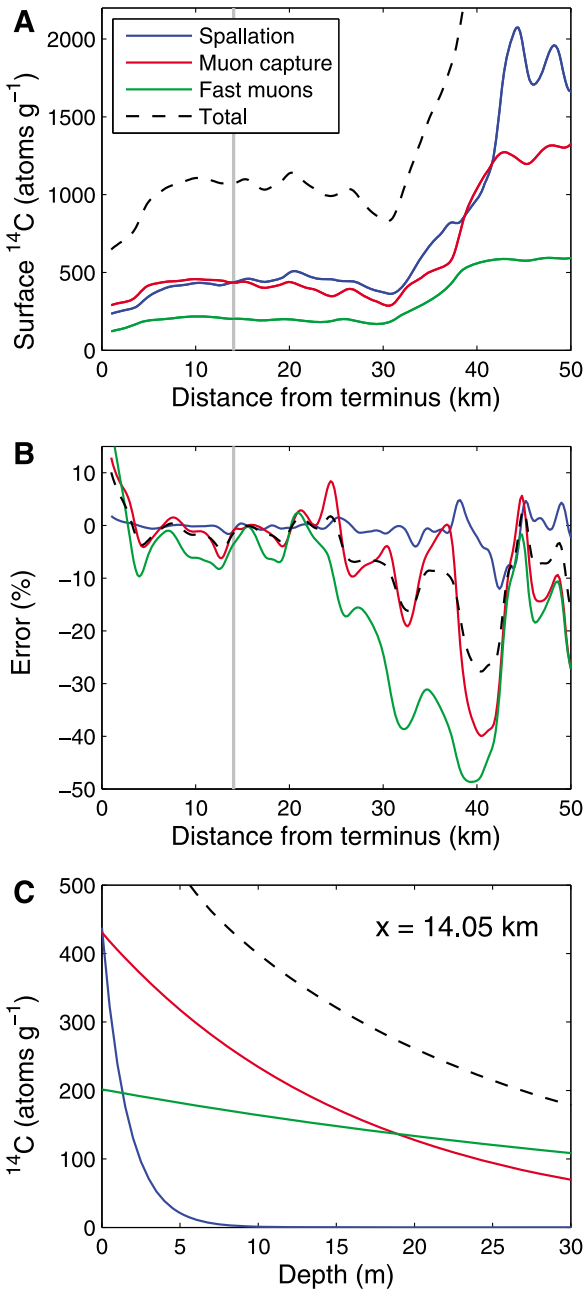

Figure 7. (a) Modeled surface cosmogenic ^{14}C concentration (atoms g^{-1}) for the three production mechanisms. The black dashed line gives the total concentration, i.e., the sum of the three individual mechanisms. (b) Error when using the ablation-only approximation of equation (12), expressed as a percentage of the full 2-D model solution. Negative values means that the ablation-only approximation underestimates the true in situ production. (c) Depth profile of ^{14}C concentration for the three production mechanisms at the sampling site of the 2010/2011 field campaign, x = 14.05 km.

2010/2011 sampling site was selected to have an ice age >50 ka [*Aciego et al.*, 2007], meaning that effectively all the ^{14}C inherited from the paleo-atmosphere and cosmogenic production in the accumulation zone has decayed. Furthermore, we are interested in the ablation signal only. For these reasons we let the inheritance $A_i = 0$; all ice parcels start with zero ^{14}C activity at the upstream edge of the model (x = 72.4 km) at all depths. To avoid any artifacts originating from the model domain edge we only use results for $x < 50$ km. The calculated concentrations are shown in Figure 7a. As we get further away from the terminus, the signal increases due to an enhanced cosmogenic surface production with greater altitude, as well as lower ablation rates. Around x = 30 km there is a local minimum in the ^{14}C concentration, which is due to the katabatic wind-induced ablation rate maximum referred to earlier.

[32] We can compare our calculated surface values to the estimate given by *Lal et al.* [1990]:

$$[^{14}\mathrm{C}]_i(z) = \frac{P_i^0 e^{\rho z/\Lambda_i}}{\rho a/\Lambda_i + \lambda} \tag{12}$$

where a is the ablation rate $a = -\dot{b}$. This double notation is chosen to be consistent with notation used in both glaciological and cosmogenic nuclide literature. Note that equation (12) neglects the effects of strain rates and lateral flow. We shall refer to equation (12) as the ablation-only approximation. Figure 7b shows the error introduced when using this approximation, expressed as a percentage of the full 2-D trajectory modeling solution. The spallogenic component is only sensitive to ice flow in the top ~20 m; consequently, there is not much difference between the trajectory modeling and the ablation-only approximation (as both use identical vertical ice velocity at the surface). The muogenic nuclide production deviates more strongly from the ablation-only case, as it also occurs at greater depths. Near the overdeepening at x = 40 km, the fast muon production differs by up to 50% from ablation-only. Because ice parcels come from greater altitudes (and therefore higher production rates) upstream, the ablation-only approximation tends to underestimate nuclide production. Our 2010/2011 ^{14}C sampling site at x = 14.05 km (indicated by the vertical grey line) lies at a position where the deviation from the ablation-only case is near a minimum; when using equation (12) to interpret data, an error of ~5% is introduced.

[33] Several previous studies have used ^{14}C concentrations in combination with equation (12) to estimate ablation rates in glaciers and BIAs [e.g., *Lal et al.*, 1990; *Van Roijen et al.*, 1995; *Van der Borg et al.*, 2001]. Our modeling results show that neglecting the flow history of the ice parcels can result in an error of up to 25% where topography is rugged (black dashed line in Figure 7b); the proximity of many Antarctic BIAs to mountain ranges and nunataks [*Bintanja*, 1999; *Sinisalo and Moore*, 2010] suggests that caution is warranted when estimating ablation rates from radiocarbon data.

[34] Ice samples for gas analysis should be taken from several meter below the surface, where they are less likely to be compromised by gas exchange with the modern atmosphere through (thermal) surface cracks. Figure 7c shows the depth profiles of the different production mechanisms at the sampling site. Below ~6 m depth the spallogenic component is nearly absent; samples taken at these depths should allow us to determine the muogenic production rates more accurately than the current laboratory estimates (Table 1).

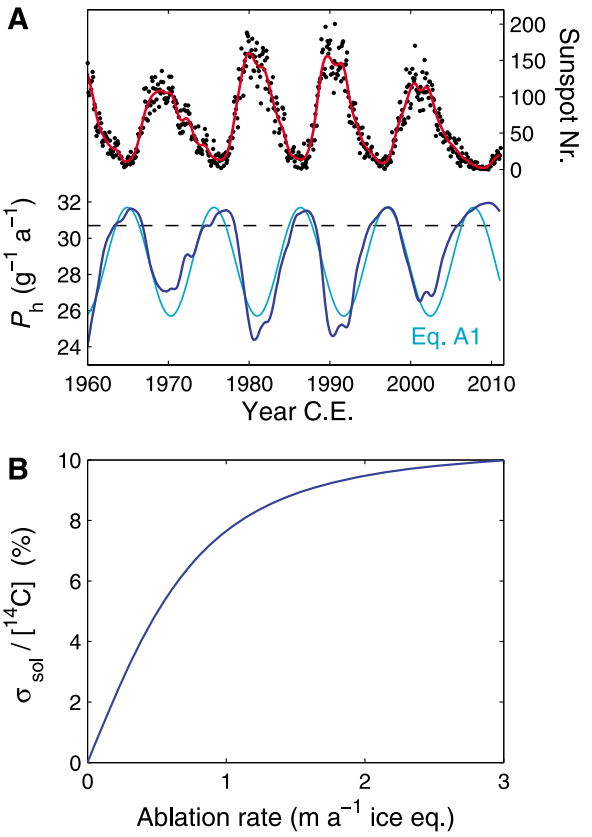

Figure 8. (a) Right axis: observational record of monthly averaged sunspot numbers (ftp://ftp.ngdc.noaa.gov/STP/SOLAR_DATA/SUNSPOT_NUMBERS/INTERNATIONAL/monthly/, black dots), together with a 1 year running average (red line). Left axis: Spallogenic surface production rate estimate using the *Lifton et al.* [2005] scaling model at high latitude ($R_C \leq 1.9$) and sea level (dark blue), and the simplified surface production rate of equation (A1) (light blue, marked). The dashed line shows the long term (11.4 ka) average production rate as given in Table 1, corresponding to a measure of solar modulation $S = 0.950$ in the *Lifton et al.* [2005] scaling model. (b) Uncertainty in spallogenic production as a function of the ablation rate a given by equation (13), expressed as a percentage of total spallogenic production.

4.2. Solar Modulation of the Cosmic Ray Flux

[35] We will now examine how solar modulation of the cosmic ray flux affects the ^{14}C content of ablating ice parcels. Variations in solar activity mostly influence low energy cosmic rays, while high energy rays are less affected [*Lifton et al.*, 2005, and references therein]. At the high latitudes of our study site the geomagnetic field provides little shielding. Thus effectively all cosmic rays are admitted, including the low energy rays that are modulated by solar activity. Consequently variations in solar activity should be considered when studying cosmogenic production in polar regions. Note that spallogenic production is most sensitive to solar modulation; muons are produced by incoming primary cosmic ray particles of higher median energies, which are not affected by solar modulation. The scaling model by *Lifton et al.* [2005] incorporates solar activity by relating cosmic ray intensity to sunspot numbers, of which there is an observational record dating back to the 17th century [*Hoyt and Schatten*, 1998]. Following *Lifton et al.* [2005], the tree ring ^{14}C-based sunspot number reconstruction by *Solanki et al.* [2004] is used prior to the existing observational record. Only spallogenic production rates are sensitive to solar modulation in the scaling model.

[36] Figure 8a shows the changes in the spallogenic ^{14}C surface production rate for the last 4 solar cycles at sea level and high latitude (i.e., any site with $R_C \leq 1.9$, our model uses $R_C = 0$). Production is lowest during periods of high solar activity. The dashed line represents the long term average production rate as given in Table 1.

[37] How much these variations influence the ^{14}C content of an ice parcel depends on the ablation rate. In appendix A we derive an analytical expression for the relative uncertainty $\sigma_{sol}/[^{14}C]_h$ in the spallogenic production term as a function of ablation rate:

$$\frac{\sigma_{sol}}{[^{14}C]_h} \approx \frac{\kappa}{k} \frac{\frac{\rho a}{\Lambda_h}}{\sqrt{\left(\frac{2\pi}{\tau}\right)^2 + \left(\frac{\rho a}{\Lambda_h}\right)^2}} \tag{13}$$

How the uncertainty σ_{sol} changes as a function of a is plotted in Figure 8b, expressed as a percentage of total $[^{14}C]_h$. For Taylor Glacier (a = 0.1–0.3 m a^{-1}) the influence of solar modulation is relatively small. The reason is that ice parcels are exposed to several sunspot cycles on their way to the surface, causing the variations to average out. Solar modulation should be considered at Greenlandic high ablation sites such as Pakitsoq, where annual rates of ~2.5 m a^{-1} can be found [*Reeh et al.*, 2002; *Petrenko et al.*, 2009]. At such sites the ice parcels are transported through the exposed top ~5 m over a time interval much shorter than the duration of a sunspot cycle, causing a 10 % variation with time. At these sites the sampling date should be taken into account when analyzing ^{14}C data.

[38] Solar modulation mostly influences the spallogenic production. Cosmogenic ^{14}C production at depths $z > 5$ m is dominated by muogenic production, and therefore less sensitive to solar activity (and thereby sampling date). Consequently, for ablation sites solar modulation can be neglected at $z > 5$ m. For accumulation sites the solar variations in nuclide production are transported into the ice, and should always be considered when accumulation rates are high.

4.3. Sensitivity of Results to the Main Sources of Uncertainty

[39] Although solar modulation does not play a major role at Taylor Glacier, the modeled ^{14}C concentrations are subject to a number of other uncertainties. We present a sensitivity study comparing the magnitude of potential errors, the results of which are shown in Figures 9a–9c. The colors in the figure correspond to different sampling depths in the ice. We look at both the surface concentrations, as well as concentrations at depths which are more suited for gas measurements (i.e., ice not subjected to gas exchange through near-surface cracks, commonly observed at BIAs).

[40] We analyze the three main sources of uncertainty: (1) the choice of strain rate parameterization, (2) the ablation rate estimate based on measurements from a limited number

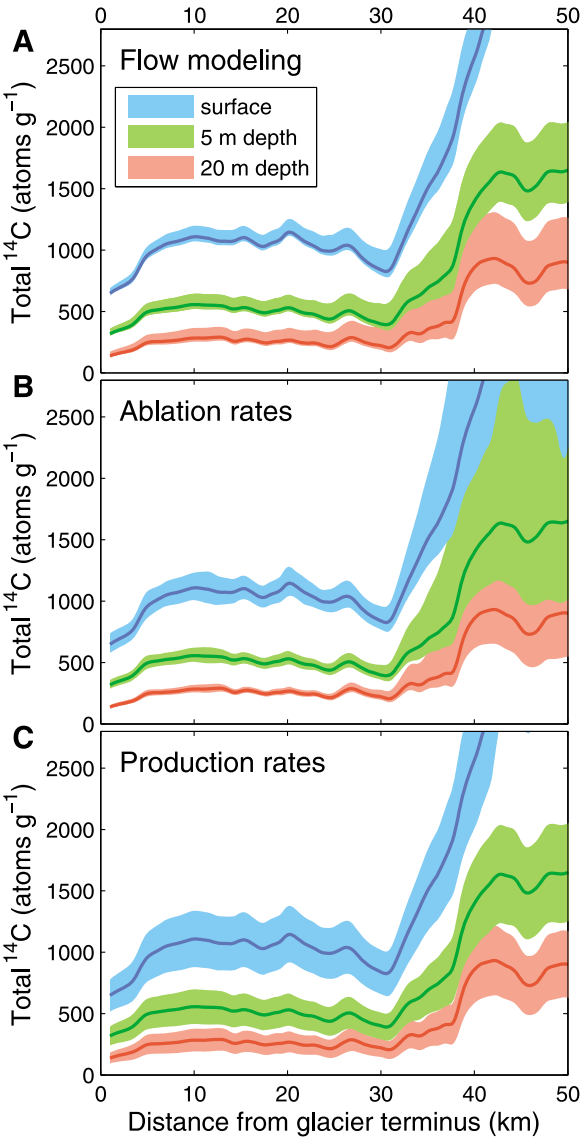

Figure 9. (a) Uncertainty in the strain rate parameterization. For each point along x, and at the indicated depths, we evaluated three potential back-trajectories; our best estimate trajectory (solid curve) and the two enveloping highest- and lowest-elevation trajectories of Figure 5c (shaded region). (b) Uncertainty in the ablation rate estimate as shown in Figure 5a. Modeled ^{14}C concentrations using our best estimate ablation rates (solid curve) and using ablation rates of $a \pm 1\sigma_a$ (envelope to shaded region). (c) Uncertainties due to the cosmogenic production rates found in literature, as summarized in Table 1. Modeled ^{14}C concentrations using the published production rates (solid curve) and using production rates of $P_i^0 \pm 1\sigma_i$ (envelope to shaded region).

of years, and (3) uncertainty in the cosmogenic production rates as found in literature. For each plot the darker central lines give our modeled best estimate total cosmogenic ^{14}C concentrations, whereas the shaded areas give the uncertainty estimate. In our discussion of the sensitivity study we focus on the part of the glacier where $x < 35$ km, which is the part that exposes the oldest ice, and is therefore most interesting for paleo-climate reconstructions [*Aciego et al.*, 2007].

[41] The uncertainty contribution of the strain rate parameterization (Figure 9a) shows little depth dependence between the surface and $z = 20$ m. This is because the strain rates mostly influence the flow at depth, whereas the near-surface trajectories are fixed by the ablation rate and are only minorly influenced by strain rate uncertainties. The fact that the best estimate solution does not lie in the middle of the uncertainty band, but rather at the lower end, results from the exponential depth dependence of the nuclide production.

[42] As long as the ablation uncertainty σ_a is small relative to the ablation rate a, the resulting uncertainty in ^{14}C production is expected to be proportional to the amount of production itself as per equation (12). This is what is indeed observed for $x < 35$ km where a is large (Figure 9b). As σ_a approaches a (i.e., for $x > 35$ km), the uncertainty in ^{14}C increases rapidly with increasing x.

[43] For all depths considered, the nuclide production rates as found in literature are the largest source of uncertainty. In particular, the fast muon production rate has a large uncertainty of about 60% (Table 1). As shown in Figure 7c, the spallation component is insignificant below 5 m depth. This implies that the deeper samples (5–20 m) collected at Taylor Glacier for ^{14}C analyses during the 2010/2011 season would allow us to improve substantially on the current estimates for muogenic ^{14}C production from ^{16}O. Such improved production estimates would be important not just for studies of ^{14}C in ice, but for cosmogenic studies of other materials, such as e.g., quartz and carbonate rocks commonly used in exposure dating [*Gosse and Phillips*, 2001].

5. Summary and Conclusions

[44] In this work we investigated in situ cosmogenic ^{14}C production at ablation sites. First, we implemented a thermal neutron flux model for the air-ice interface, and found that thermal neutron capture by nitrogen in air bubbles produces only negligible amounts of ^{14}C.

[45] Second, by modeling the trajectories of ice parcels at the center line of Taylor Glacier we calculated a best-estimate ^{14}C concentration of ablating ice. We found that the commonly used ablation-only approximation by *Lal et al.* [1990] tends to underestimate production as the ice flows down from parts of the glacier that have higher production rates. For sections of the glacier where the basal topography is rugged, the ablation-only approximation deviates from the full model solution by up to 25%. This has important consequences when ^{14}C measurements are used to estimate ablation rates.

[46] Third, we demonstrated that the influence of solar modulation is strongly dependent on ablation rate. At low ablation sites, such as Taylor Glacier, the effect is small due to temporal averaging over several sunspot cycles. At high ablation sites, such as Pakitsoq, Greenland, solar modulation introduces an uncertainty of up to 10% in the spallogenic component. In these cases the sampling date needs to be considered when interpreting data.

[47] We introduced two methods to parameterize vertical strain rates with depth. The first method is based on conservation of mass in the ice column; the second method is based on measured surface strain rates. The second method proved to be less reliable, because (1) estimated surface

strain rates from InSAR and GPS measurements show a poor correlation, (2) flow lines do not follow bedrock, and (3) mass is not conserved.

[48] We presented a sensitivity study where we compared potential errors introduced by uncertainties in the strain rate parameterization, the ablation rates, and the published cosmogenic production rates. We found that the cosmogenic production rates are the largest source of uncertainty. In the 2010/2011 austral summer, Taylor Glacier ice was sampled with the aim of constraining the cosmogenic production rates more strongly. By sampling at depths >5 m the muogenic components can be isolated, which have the largest uncertainty in their production rates. The modeling results presented here will aid us with the interpretation of ^{14}C measurements on these samples.

Appendix A: Derivation of Equation (13)

[49] For simplicity we assume a sinusoidal solar modulation of the spallogenic surface production

$$P_h^0 = k + \mathbf{Re}\{\kappa \exp(2i\pi t/\tau + i\theta)\} \tag{A1}$$

where τ = 11 yr is the period of the sunspot (or Schwabe) cycle, θ is the phase of the cycle, $k = 28.7$ and $\kappa = 3$ are fitted by eye to the modeled production rate curve, and $\mathbf{Re}\{.\}$ denotes the real part of the expression. The simplified production of equation (A1) is plotted in Figure 8a, together with the modeled production. Ignoring inheritance and radioactive decay, the spallogenic ^{14}C in an ice parcel that ablates at the glacier surface at $t = 0$ is given by

$$[^{14}\mathrm{C}]_h(z) = \mathbf{Re}\left\{ \int_{-\infty}^{-z/a} \left[k + \kappa \exp\left(\frac{2i\pi t}{\tau} + i\theta \right) \right] \exp\left(\frac{\rho a t}{\Lambda_h} \right) dt \right\} \tag{A2}$$

Note that this equation also holds for the accumulation zone, in which case the integral goes from 0 to z/a, and a is replaced by $-a$ in the integrand. The solution at the surface is given by

$$[^{14}\mathrm{C}]_h(0) = \frac{k}{\frac{\rho a}{\Lambda_h}} + \frac{\kappa \sin(\theta + \varphi)}{\sqrt{\left(\frac{2\pi}{\tau}\right)^2 + \left(\frac{\rho a}{\Lambda_h}\right)^2}} \tag{A3}$$

with

$$\varphi = \arcsin\left(\frac{\rho a}{\Lambda_h} \Big/ \sqrt{\left(\frac{2\pi}{\tau}\right)^2 + \left(\frac{\rho a}{\Lambda_h}\right)^2} \right) \tag{A4}$$

The first term in equation (A3) gives the time-invariant long-term average ^{14}C concentration; the second term gives the time (i.e., θ) dependent part caused by solar modulation. When solar variation is neglected in the analysis of ^{14}C data, the phase θ of the sunspot cycle is not fixed, and an uncertainty σ_{sol} is introduced. On dividing the second term in equation (A3) by the first term we obtain for the relative uncertainty:

$$\frac{\sigma_{\mathrm{sol}}}{[^{14}\mathrm{C}]_h} \approx \frac{\kappa}{k} \frac{\frac{\rho a}{\Lambda_h}}{\sqrt{\left(\frac{2\pi}{\tau}\right)^2 + \left(\frac{\rho a}{\Lambda_h}\right)^2}} \tag{A5}$$

[50] **Acknowledgments.** We would like to thank Andy Bliss for his help on calculating ablation rates, Daniel Baggenstos for measuring ablation stakes in the field and providing locations of the 2009–2010 sampling transect, Brent Goehring for fruitful discussions, and Tom Neumann for many constructive comments on the manuscript. C. Buizert would like to thank Thomas Blunier (Center for Ice and Climate, University of Copenhagen), Bruce Vaughn and Jim White (INSTAAR, University of Colorado) for their support and hospitality; V. V. Petrenko has been supported by the NOAA Postdoctoral Fellowship in Climate and Global Change, NSF grants 0632222 and 0806387 (White) and NSF grant 0839031 (Severinghaus); this work was partially supported by NSF grant OPP-0125579 to K. M. Cuffey and NSF grant 0838936 to E. J. Brook; N. A. Lifton is grateful for support by the CRONUS-Earth project (NSF EAR0345150) and the University of Arizona Accelerator Mass Spectrometry Laboratory.

References

Aciego, S. M., K. M. Cuffey, J. L. Kavanaugh, D. L. Morse, and J. P. Severinghaus (2007), Pleistocene ice and paleo-strain rates at Taylor Glacier, Antarctica, *Quat. Res.*, *68*, 303–313.

Andree, M., et al. (1984), ^{14}C dating of polar ice, *Nucl. Instrum. Methods Phys. Res., Sect. B*, *5*(2), 385–388.

Azuma, N., M. Nakawo, A. Higashi, and F. Nishio (1985), Flow pattern near massif a in the yamato bare ice field estimated from the structures and the mechanical properties of a shallow ice core, *Mem. Natl. Inst. Polar Res., Spec. Issue Jpn.*, *39*, 173–183.

Bintanja, R. (1999), On the glaciological, meteorological, and climatological significance of Antarctic blue ice areas, *Rev. Geophys.*, *37*(3), 337–359.

Bliss, A. K., K. M. Cuffey, and J. L. Kavanaugh (2011), Sublimation and surface energy budget of Taylor Glacier, Antarctica, *J. Glaciol.*, *57*(204), 684–696.

Cuffey, K., and W. S. B. Paterson (2010), *The Physics of Glaciers*, 4th ed., Elsevier, Burlington, Mass.

De Jong, A., C. Alderliesten, K. Van der Borg, C. Van der Veen, and R. Van De Wal (2004), Radiocarbon analysis of the EPICA Dome C ice core: No in situ ^{14}C from the firn observed, *Nucl. Instrum. Methods Phys. Res., Sect. B*, *223*, 516–520.

Desilets, D., and M. Zreda (2003), Spatial and temporal distribution of secondary cosmic-ray nucleon intensities and applications to in situ cosmogenic dating, *Earth Planet. Sci. Lett.*, *206*(1–2), 21–42.

Desilets, D., M. Zreda, and T. Prabu (2006), Extended scaling factors for in situ cosmogenic nuclides: New measurements at low latitude, *Earth Planet. Sci. Lett.*, *246*(3–4), 265–276.

Dunai, T. J. (2000), Scaling factors for production rates of in situ produced cosmogenic nuclides: A critical reevaluation, *Earth Planet. Sci. Lett.*, *176*, 157–169.

Dunbar, N. W., W. C. McIntosh, and R. P. Esser (2008), Physical setting and tephrochronology of the summit caldera ice record at Mount Moulton, West Antarctica, *Geol. Soc. Am. Bull.*, *120*(7–8), 796–812.

Fireman, E., and T. Norris (1982), Ages and composition of gas trapped in Allan-Hills and Byrd core ice, *Earth Planet. Sci. Lett.*, *60*(3), 339–350.

Gosse, J. C., and F. M. Phillips (2001), Terrestrial in situ cosmogenic nuclides: Theory and application, *Quaternary Sci. Rev.*, *20*, 1475–1560.

Grinsted, A., J. Moore, V. B. Spikes, and A. Sinisalo (2003), Dating Antarctic blue ice areas using a novel ice flow model, *Geophys. Res. Lett.*, *30*(19), 2005, doi:10.1029/2003GL017957.

Heisinger, B., D. Lal, A. J. T. Jull, P. Kubik, S. Ivy-Ochs, K. Knie, and E. Nolte (2002a), Production of selected cosmogenic radionuclides by muons: 2. Capture of negative muons, *Earth Planet. Sci. Lett.*, *200*(3–4), 357–369.

Heisinger, B., D. Lal, A. J. T. Jull, P. Kubik, S. Ivy-Ochs, S. Neumaier, K. Knie, V. Lazarev, and E. Nolte (2002b), Production of selected cosmogenic radionuclides by muons: 1. Fast muons, *Earth Planet. Sci. Lett.*, *200*(3–4), 345–355.

Hoyt, D. V., and K. H. Schatten (1998), Group sunspot numbers: A new solar activity reconstruction, *Sol. Phys.*, *181*, 491–491.

Jenk, T. M., S. Szidat, M. Schwikowski, H. W. Gaeggeler, L. Wacker, H.-A. Synal, and M. Saurer (2007), Microgram level radiocarbon ^{14}C) determination on carbonaceous particles in ice, *Nucl. Instrum. Methods Phys. Res., Sect. B*, *259*(1), 518–525.

Jouzel, J., et al. (2007), Orbital and millennial antarctic climate variability over the past 800,000 years, *Science*, *317*(5839), 793–796.

Kavanaugh, J. L., and K. M. Cuffey (2009), Dynamics and mass balance of Taylor Glacier, Antarctica: 2. Force balance and longitudinal coupling, *J. Geophys. Res.*, *114*, F04011, doi:10.1029/2009JF001329.

Kavanaugh, J. L., K. M. Cuffey, D. L. Morse, H. Conway, and E. Rignot (2009a), Dynamics and mass balance of Taylor Glacier, Antarctica:

1. Geometry and surface velocities, *J. Geophys. Res.*, *114*, F04010, doi:10.1029/2009JF001309.

Kavanaugh, J. L., K. M. Cuffey, D. L. Morse, A. K. Bliss, and S. M. Aciego (2009b), Dynamics and mass balance of Taylor Glacier, Antarctica: 3. State of mass balance, *J. Geophys. Res.*, *114*, F04012, doi:10.1029/2009JF001331.

Lal, D. (1991), Cosmic-ray labeling of erosion surfaces: In situ nuclide production-rates and erosion models, *Earth Planet. Sci. Lett.*, *104*(2–4), 424–439.

Lal, D., K. Nishiizumi, and J. R. Arnold (1987), In situ cosmogenic ^{3}H, ^{14}C, and ^{10}Be for determining the net accumulation and ablation rates of ice sheets, *J. Geophys. Res.*, *92*(B6), 4947–4952.

Lal, D., A. J. T. Jull, D. J. Donahue, D. Burtner, and K. Nishiizumi (1990), Polar ice ablation rates measured using in situ cosmogenic ^{14}C, *Nature*, *346*(6282), 350–352.

Lal, D., A. J. T. Jull, G. S. Burr, and D. J. Donahue (2000), On the characteristics of cosmogenic in situ ^{14}C in some GISP2 Holocene and late glacial ice samples, *Nucl. Instrum. Methods Phys. Res., Sect. B*, *172*, 623–631.

Lal, D., A. Jull, D. Donahue, G. Burr, B. Deck, J. Jouzel, and E. Steig (2001), Record of cosmogenic in situ produced C-14 in Vostok and Taylor Dome ice samples: Implications for strong role of wind ventilation processes, *J. Geophys. Res.*, *106*(D23), 31,933–31,941.

Lifton, N. A., J. W. Bieber, J. M. Clem, M. L. Duldig, P. Evenson, J. E. Humble, and R. Pyle (2005), Addressing solar modulation and long-term uncertainties in scaling secondary cosmic rays for in situ cosmogenic nuclide applications, *Earth Planet. Sci. Lett.*, *239*, 140–161.

Liu, B., F. M. Phillips, J. T. Fabryka-Martin, M. M. Fowler, and W. D. Stone (1994), Cosmogenic ^{36}Cl accumulation in unstable landforms: 1. Effects of the thermal neutron distribution, *Water Resour. Res.*, *30*(11), 3115–3125.

Moore, J. C., F. Nishio, S. Fujita, H. Narita, E. Pasteur, A. Grinsted, A. Sinisalo, and N. Maeno (2006), Interpreting ancient ice in a shallow ice core from the South Yamato (Antarctica) blue ice area using flow modeling and compositional matching to deep ice cores, *J. Geophys. Res.*, *111*, D16302, doi:10.1029/2005JD006343.

Mughabghab, S., M. Divadeenam, and N. E. Holden (1992), *Neutron Resonance Parameters and Thermal Cross Sections*, Academic, New York.

Nesterenok, A. V., and V. O. Naidenov (2009), Radiocarbon in the antarctic ice: The formation of the cosmic ray muon component at large depths, *Geomagn. Aeronomy*, *50*, 134–140.

Petrenko, V., J. Severinghaus, E. Brook, N. Reeh, and H. Schaefer (2006), Gas records from the West Greenland ice margin covering the Last Glacial Termination: A horizontal ice core, *Quaternary Sci. Rev.*, *25*(9–10), 865–875.

Petrenko, V. V., et al. (2008), A novel method for obtaining very large ancient air samples from ablating glacial ice for analyses of methane radiocarbon, *J. Glaciol.*, *54*(185), 233–244.

Petrenko, V. V., et al. (2009), $^{14}CH_4$ measurements in Greenland ice: Investigating last glacial termination CH_4 sources, *Science*, *324*, 506–508.

Phillips, F. M., W. D. Stone, and J. T. Fabryka-Martin (2001), An improved approach to calculating low-energy cosmic-ray neutron fluxes near the land/atmosphere interface, *Chem. Geol.*, *175*(3–4), 689–701.

Reeh, N., H. Oerter, and H. Thomsen (2002), Comparison between Greenland ice-margin and ice-core oxygen-18 records, *Ann. Glaciol.*, *35*, 136–144.

Schaefer, H., V. V. Petrenko, E. J. Brook, J. P. Severinghaus, N. Reeh, J. R. Melton, and L. Mitchell (2009), Ice stratigraphy at the Pakitsoq ice margin, West Greenland, derived from gas records, *J. Glaciol.*, *55*(191), 411–421.

Sears, V. F. (1992), Neutron scattering lengths and cross sections, *Neutron News*, *3*(3), 26–37.

Sinisalo, A., and J. C. Moore (2010), Antarctic blue ice areas: Towards extracting palaeoclimate information, *Antarct. Sci.*, *22*(2), 99–115.

Smith, A. M., V. A. Levchenko, D. M. Etheridge, D. C. Lowe, Q. Hua, C. M. Trudinger, U. Zoppi, and A. Elcheikh (2000), In search of in-situ radiocarbon in law dome ice and firn, *Nucl. Instrum. Methods Phys. Res., Sect. B*, *172*, 610–622.

Solanki, S., I. Usoskin, B. Kromer, M. Schüssler, and J. Beer (2004), Unusual activity of the Sun during recent decades compared to the previous 11,000 years, *Nature*, *431*(7012), 1084–1087.

Stone, J. O. (2000), Air pressure and cosmogenic isotope production, *J. Geophys. Res.*, *105*(B10), 23,753–23,759.

Van der Borg, K., W. Van der Kemp, C. Alderliesten, A. De Jong, and R. Lamers (2001), In-situ radiocarbon production by neutrons and muons in an antarctic blue ice field at Scharffenbergbotnen: A status report, *Radiocarbon*, *43*, 751–757.

Van Der Kemp, W., C. Alderliesten, K. Van Der Borg, A. De Jong, R. Lamers, J. Oerlemans, M. Thomassen, and R. Van De Wal (2002), In situ produced ^{14}C by cosmic ray muons in ablating Antarctic ice, *Tellus B*, *54*(2), 186–192.

Van de Wal, R., J. Van Roijen, D. Raynaud, K. Van der Borg, A. De Jong, J. Oerlemans, V. Lipenkov, and P. Huybrechts (1994), From $^{14}C^{12}C$ measurements towards radiocarbon dating of ice, *Tellus B*, *46*(2), 94–102.

Van de Wal, R. S. W., H. A. J. Meijer, M. De Rooij, and C. Van der Veen (2007), Radiocarbon analyses along the EDML ice core in Antarctica, *Tellus B*, *59*(1), 157–165.

Van Roijen, J., K. Van der Borg, A. De Jong, and J. Oerlemans (1995), A correction for in-situ ^{14}C in Antarctic ice with ^{14}CO, *Radiocarbon*, *37*, 165–169.

Wagemans, J., C. Wagemans, G. Goeminne, and P. Geltenbort (2000), Experimental determination of the $^{14}n(n, p)^{14}c$ reaction cross section for thermal neutrons, *Phys. Rev. C*, *61*(6), 064601, doi:10.1103/PhysRevC.61.064601.